Kinetic Study on the CO_2 Gasification of Biochar Derived from Miscanthus at Different Processing Conditions

Hong Tian [1, 2], Qingsong Hu [1], Jiawei Wang [2], Donglin Chen [1], Yang Yang [2]*, Anthony V. Bridgwater [2]

[1] *School of Energy & Power Engineering, Changsha University of Science & Technology, Changsha 410114, China*

[2] *Bioenergy Research Group, EBRI, Aston University, Birmingham B4 7ET, UK.*

Corresponding author: Y. Yang y.yang6@aston.ac.uk; +44 (0) 121 204 3433

ABSTRACT

CO_2 gasification is an emerging process that can improve the quality of syngas and enhance the CO_2 circular utilisation. This paper presents an analysis on the CO_2 gasification of Miscanthus-derived biochar produced at various processing conditions. The gasification behaviour, kinetics and biochar reactivity were investigated and the correlations to the biochar preparation condition and their microstructure were developed. Results showed that the preparation and gasification reaction conditions had major impact on the biochar reactivity. The order of significance that affected the biochar reactivity was gasification temperature, biochar preparation temperature and processing atmosphere. Increasing heating rate could enhance the biochar reactivity, while increasing preparation temperature could reduce the reactivity in N_2 and He atmosphere. At 600 and 1000 °C, He atmosphere produced the most activity biochar, followed by N_2 and CO_2. At 800 °C, CO_2 atmosphere gave the highest reactivity, followed by He and N_2. The Activation Energy (*E*) of gasification reaction calculated by the Hybrid Model was mainly in the range of 78.09-212.46 kJ mol^{-1}. The *E* decreased with the increase of carbon conversion rate. A great kinetic compensation effect between *E* and *A* was identified during the CO_2 gasification process.

Keyword: Biochar Processing; Biochar Reactivity; Pyrolysis; CO2 Gasification; Kinetic Modelling

1. INTRODUCTION

Biomass is an important renewable energy source, as it is widely available and accessible and is the only renewable carbon source on earth. The development of bioenergy industry improves the energy independence and security. The increasing demand for bioenergy has driven development of the energy crops. Miscanthus is a perennial herb with C4 photosynthesis, which has been considered as one of the most potential renewable energy crop due to its fast growth rate, high yield (the annual output of about 27-44 tons per hectare), high cellulose content (43.1-52.2 wt.%), remarkable adaptability to different environments, disease resistance and low production cost [1, 2].

Biochar is the solid product from the pyrolysis of biomass with largely improved characteristics comparing to the raw material in solid fuel application. Carefully prepared biochar product usually has a rich pore structure, low volatile, high heating value and good electrical conductivity. Biochar is essentially used as a solid fuel, but also has applications in agriculture and materials development [3, 4]. For typical intermediate and slow pyrolysis processes, the productivity usually accounts for around 30-50 wt.% of the total products [5].

Despite the influence from the raw material, the characteristics of the biochar product largely vary with the processing conditions (i.e. temperature, heating rate, atmospheres, etc.) [6, 7]. During the biochar preparation process, manipulating the processing atmosphere, for example switch between the inert environment (N_2, He) and the reactive environment (CO_2) could affect the biochar's microstructure, porosity and reactivity [6, 8]. It is reported that CO_2 assisted gasification resulted in product with much higher surface area than those produced in N_2 atmosphere [8, 9]. Wang et al. [6] studied the structure of corncob derived biochar prepared at a variety of atmospheres (i.e. N_2, H_2, CO and CO_2). The results showed that the atmosphere affect structure and the physicochemical properties of the biochar. Under the same preparation temperature, the

order of the biochar specific surface area was CO_2, H_2, N_2 and CO (from high to low). The ordering degree of biochar obtained under the four atmospheres from high to low was N_2, CO_2, CO and H_2. Fan et al. [10] analysed the walnut shell derived char prepared in N_2, O_2 and CO_2 atmospheres. It was found that CO_2 had an activation effect, which resulted in the product having very high specific area and adsorption capacity. It was interesting to find that O_2 could result in the formation of oxygen-containing functional groups (such as carboxyl and carbonyl groups) on the surface of the biochar. In addition, biochar preparation temperature had a major impact on the structure of biochar. Some studies showed that when the biochar preparation temperature increased, the surface carbonaceous structure of biochar was gradually destroyed and most of the surface functional groups vanished, the microcrystalline of biochar was more orderly and regularised [11, 12]. Biochar gasification with CO_2 as the gasifying agent could consume CO_2 to produce syngas, which realised the carbon circular utilisation. Developing CO_2 assisted gasification have become a topic of great interest recently, and there have been a number of works addressed the research in this process, which demonstrated the process feasibility and identified the opportunity for further development [13-17] .

Gasification reactivity and reaction kinetics of biochar has been studied in the past years. Nevertheless, the gasification reactivity is very difficult to predict because of the difference in their physicochemical properties. Tian et al. [18] reported that the microcrystalline structure and the alkali and alkaline earth metal content in the miscanthus derived biochar were the dominant factors for the change of gasification reactivity. Fatehi et al. [19] indicated the evolution of biochar porosity could affect the rate of thermal conversion of the biochar by affecting the intraparticle transport. It was also identified the increase in the effective surface area led to an increased gasification reactivity of biochar during the entire conversion process. Wu et al. [20] investigated the influencing mechanism of organic alkali metal on biochar structure evolution and gasification

reactivity. It was found that the low ordering of biochar structure and the evolution of organic sodium led to high reactivity and low activation energy during the gasification process. From the above literatures, it can be found that, there is no certain factor identified for evaluating the gasification reactivity of different biochar materials. In order to investigate the difference in gasification reactivity of Miscanthus-derived biochar prepared at different processing atmospheres, an acceptable factor should be found.

Gasification of biomass generally contains in two stages: 1) pyrolysis of the feedstock to produce volatiles and biochar, and 2) secondary cracking of volatile matters and gasification of biochar to produce syngas. The biochar gasification is the committed step, which is due to its low conversion rate and higher activation energy compared to the raw material pyrolysis stage [21]. The reaction kinetics are critical in process development, as they provide important parameters for reactor design and process modelling [22]. Some research showed that the kinetic parameters of different biochar produced by different conditions are not the same [3, 18, 23]. Wang et al. [6] obtained the CO_2 gasification kinetic parameters of biochar prepared at N_2, H_2, CO and CO_2 atmosphere by a number of kinetic modelling methods. It was found that the activation energy for the biochar produced in N_2, H_2, CO and CO_2 were in the range of 224.9-248.8, 228.9-258.1, 221.4-255.9 and 223.2-249.8 kJ mol^{-1}, respectively. This revealed that the activation energy of biochar obtained under different production atmosphere was highly similar. Tong et al. [7] proposed that the activation energy of biochar increased when the temperature was high. The Ortega method (The actual kinetics of a solid-state reaction cannot be discerned by means of the kinetic analysis of a single thermogravimetric curve. The TG curve calculated using a linear heating programme by assuming a particular kinetic law [24, 25]) proved that F2 mechanism applied to the gasification of biochar at lower biochar preparation temperature, while the F1 mechanism was applied at higher

biochar preparation temperature. This indicated that the biochar preparation temperature had a great impact on kinetic parameters and reaction mechanism of biochar gasification.

In our previously work [18], it was discovered that the biochar preparation temperature resulted in significant differences in material microstructure, composition, and gasification reactivity of the biochar prepared at N_2 atmospheres. In order to further study the microstructure characteristic and gasification reactivity of biochar for optimisation, it is important to comprehensively understand the parametric factors that can influence the gasification mechanism under a variety of processing atmospheres.

In the present study, the effects of the processing atmosphere and preparation temperature on the structural characteristics of Miscanthus-derived biochar were systematically investigated by a variety of characterisation and analytical methods. Analysis was conducted to correlate biochar structure and composition to the CO_2 gasification reactivity. Furthermore, the effects of gasification heating rate and temperature over the reactivity of biochar were also studied based on thermogravimetric method. Finally, the isothermal reaction kinetic data were gained by using the HM method. Meanwhile, the reaction mechanism functions of biochar CO_2 gasification were determined by using the FWO and integral master-plots method.

2. MATERIAL AND METHODS

2.1 Biochar preparation

The Miscanthus samples were collected from a local farm in Changsha, China. The Miscanthus sample was ground and fully oven dried prior to use. The Miscanthus-derived biochar was prepared at processing atmospheres of N_2, He and CO_2 under different temperatures (i.e. 600, 800 and 1000 °C) in a tube furnace. For each run, high purity processing atmosphere (100 ml min^{-1}) was initially used to purge the system for 30 minutes

in order to remove the air. The reactor was then loaded with Miscanthus samples in a sample tray and was placed in a tube furnace. Thereafter, the sample was heated at 600, 800 and 1000 °C with a heating rate of 10 °C min^{-1}, and the final preparation temperatures were kept for 60 minutes. The biochar produced at the conditions of 600, 800 and 1000 °C under N_2, He and CO_2 atmosphere were labelled as N_2-*T*, He-*T*, and CO_2-*T*, respectively (*T* being the biochar preparation temperature). The biochar samples prepared in N_2, He and CO_2 atmospheres were noted as N_2 biochar, He biochar and CO_2 biochar, respectively. The proximate and ultimate analysis of samples are shown in Table 1.

Table 1 Proximate and ultimate analysis of the Miscanthus and biochar samples

Samples	Proximate analysis [a] (wt., %)			Ultimate analysis [b] (wt., %)			
	A_d	V_d	FC_d	C	H	O[c]	N
Miscanthus	3.51	74.84	21.65	50.93	7.14	41.56	0.27
N_2-600	12.18	15.27	72.55	92.90	2.41	3.81	0.63
N_2-800	12.28	8.79	78.93	92.49	1.59	5.22	0.55
N_2-1000	12.99	8.04	78.97	91.74	2.20	5.41	0.31
He-600	12.67	13.42	73.91	89.26	3.11	6.58	0.90
He -800	13.97	8.16	77.87	89.19	2.42	7.33	0.81
He -1000	17.81	4.51	77.68	88.84	2.18	8.83	0.21
CO_2-600	11.15	10.88	77.97	90.57	3.28	4.90	0.99
CO_2-800	14.81	5.51	79.68	85.55	2.51	10.83	0.88
CO_2-1000	76.95	0.00	23.05	43.79	3.91	52.30	0.00

[a] Dry basis. [b] Dry ash-free basis. [c] Calculate by difference. FC: fixed carbon. A: ash. V: volatile matter.

2.2 Characterisation of biochar

The morphology structure of the biochar was studied by using Scanning Electron Microscopy (SEM, JSM-6060LA). The mineral elements species and content were analysed by Energy Dispersive X-ray (EDX) analysis. The pore structure and pore size distribution of biochar was analysed by N_2 adsorption (Micrometrics ASAP 2020). The specific surface area and pore size distributions of biochar was calculated by BET and BJH theory

respectively [26]. The crystal structure of the biochar was characterised by X-ray diffractometer (XRD, Rigaku Ultimate IV).

2.3 Gasification runs

The CO_2 gasification experiment analysis was carried out in a thermobalance analyser (NETZSCH, STA449F3). About 10 mg of the biochar samples were used in each test. High purity inert atmosphere (N_2, 99.999%, 20 ml min^{-1}) was employed as the purge gas. For the isothermal gasification experiment, the biochar sample was heated from ambient condition to 105 °C (at 20 °C min^{-1}) and held for 5 minutes. Then, the sample was heated at the same rate to the set conversion temperatures (i.e. 800, 900, and 1000 °C). Once the furnace reached the set gasification temperature, to the carrier gas was switched to CO_2 (100 ml min^{-1}) to create a reduction environment. The gasification condition was maintained for 120 mins. It can be seen from Table 1 that the main substance in Miscanthus-derived biochar was fixed carbon, with a little volatile and ash. The heating process before the start of isothermal gasification was carried out in nitrogen atmosphere, due to the inert protection of nitrogen, the char will not react to generate pyrolysis gas production during the heating process, but the weight of the char was slightly reduced during the heating process, which may be caused by the volatilisation of volatile substances in the char.

The non-isothermal gasification experiment followed the procedure of the isothermal runs apart from using CO_2 (80 ml min^{-1}) as the carrier gas throughout the experiment. The final temperature for non-isothermal runs were 1200 °C.

The Carbon Conversion Rate x and Gasification Rate r (min^{-1}) were calculated by using the following formula as:

$$x = (w_0 - w_t)/(w_0 - w_f) \quad (1)$$

$$r = dx/dt \quad (2)$$

where w_0 and w_f are the initial and final mass of the sample (mg), respectively; w_t is the instantaneous mass (mg) at a gasification reaction time t (min).

The quantitative description of normalised gasification rate K (min^{-1}) was employed to compare the isothermal gasification reactivity of different biochar. A high K value indicated a better gasification reactivity with shorten reaction time. The equation is as follows [27-29]:

$$K = ln4/\Delta t \quad (3)$$

where, Δt is the time of carbon conversion between 20% and 80% (min).

The quantitative description of index S was used to evaluate the effect heating rate on the reactivity of the biochar. A high S value means that the biochar has a high gasification reactivity [18].

$$S = \left(dx/dt_{max} \cdot dx/dt_{mean}\right)/T_I^2 \cdot T_f \quad (4)$$

Where, dx/dt_{max} and dx/dt_{mean} are the maximum and mean value of gasification rate (min^{-1}), respectively; T_i, T_m and T_f represent the initial conversion temperature of the samples, the temperature for peak conversion rate and the final conversion temperature of the samples (°C), respectively.

2.4 Kinetic model description

The gasification kinetic can be used to predict the complex reaction process and mechanism by analysing the gasification experiment data and provide the basis for the design and optimisation of the reaction system. As the pore structure changes during the biochar gasification reaction, the specific surface area is constantly

changing. It is hence not reasonable to define the gasification process of biochar by a single reaction model. The Hybrid Model (HM) combines the homogeneous model and shrinking core model with consideration of the empirical factors and physical parameters including reaction order and temperature. The reaction equation is expressed as [30]:

$$dx/dt = k(1-x)^n \tag{5}$$

where *n* denotes the overall reaction order. *k* represents the gasification reaction rate constant, which is only related to the reaction temperature. According to the Arrhenius law, $k = Ae^{-E/RT}$. *A* and *E* denote the pre-exponential factor (min^{-1}) and the activation energy (kJ mol^{-1}), respectively. R is the universal gas constant (8.314 J $mol\ K^{-1}$). Taken the logarithm of both sides of Eq.5, it can be expressed as:

$$ln(dx/dt) = ln\,k + n\,ln(1-x) \tag{6}$$

where $lnk = lnA - E/RT$, for a linear fit of $lnk \sim 1/T$. The *A* and *E* of gasification reaction can be obtained from the slope E/R and the intercept lnA.

The kinetics of the non-isothermal gasification process is relatively complex. The iso-conversional method determines the *E* independently on the particular mechanism that govern the transformation. The determination of *E* was a function of *x*, without assuming the reaction model. As the most common iso-conversional method, Fitlun-Wall-Ozawa (FWO) was used to derive the *E* value of the *x* from 0.1 to 0.9 [31]:

$$ln\,\beta = ln(AE/RG(x)) - 5.331 - 1.0516E/RT \tag{7}$$

where β is the heating rate (°C min^{-1}); $G(x)$ is the integral form of reaction mechanism function. The value of *E* for different conversions can be obtained from the slope of a plot of $ln\beta$ against $1000/T$.

The mechanism function of the gasification reactions was determined by the master-plots method. The mechanism function was calculated using the following equation [32]:

$$G(x) = \int_0^x \frac{dx}{f(x)} = \frac{A}{\beta}\int_{T_0}^{T} exp\left(-\frac{E}{RT}\right)dT = \frac{AE}{\beta R}[P(u) - P(u_0)] \cong P(u)AE/\beta R \quad (8)$$

$$P(u) = e^{-u}/u(1.00198882u + 1.873911198) \quad (9)$$

where $P(u)$ represents the temperature integral. $u = E/RT$.

$$G(x)/G(x_{0.5}) = P(u)/P(u_{0.5}) \quad (10)$$

where$G(x_{0.5})$, $P(u_{0.5})$ denote the value of $G(x)$ and $P(u)$at x=0.5. A series of $G(x)/G(x_{0.5}) \sim x$ theoretical master-plots curves were drawn by using various common kinetic mechanism function models $G(x)$. The experimental master-plots curves can be obtained via describing $P(u)/P(u_{0.5}) \sim x$ from the non-isothermal gasification experimental data of different biochar sample. As shown in Eq.10, in the whole range of gasification reaction, comparing the experimental value of $P(u)/P(u_{0.5})$ with the theoretical value of $G(x)/G(x_{0.5})$, the mechanism function (corresponding to the theoretical curve) that best matches the experimental curve can be considered as the most probable mechanism function of the biochar gasification reaction. It is considered that the kinetic model function $G(x)$ (corresponding to the theoretical curve) is the kinetic model function of the biochar gasification experimental curve [18].

3. RESULTS AND DISCUSSION

3.1 Characterisation of biochar

3.1.1 Biochar productivity

The biochar yield under different processing conditions are illustrated in Fig.1. It can be found that the biochar prepared in three atmospheres have the same trend that the yield reduced with the increase of preparation temperature. This is mainly due to the rearrangement of the carbon structure and the loss of hetero-atoms from the biochar which results to the decreased of biochar yield. The highest average biochar yield was in N_2, while the lowest was in CO_2 biochar. This was because the oxygen-containing functional groups (e.g. phenols, alcohols, ethers, esters etc.) had been completely decomposed in the pyrolysis process under N_2 atmosphere. The ring structure of the aromatic in biochar has been stable, resulting in the biochar yield increased. Interestingly, the biochar yield in He was about 5% lower than that in N_2 at 1000 °C. This may be related to the presence of K in the sample (shown in Table 2). The high content of potassium promote the conversion of bridges into char link, enhancing the devolatilisation rate and suppressing tar formation, leading to the higher yield of char product [33]. In addition, the He-1000 had a lower yield in comparison to the N_2-1000 due to the low volatile content (Table 1). Under the CO_2 atmosphere condition, the CO_2 can be reduced by carbon at high-temperature, which resulted in the biochar yield of CO_2-1000 was significantly lower than the yield of other biochar.

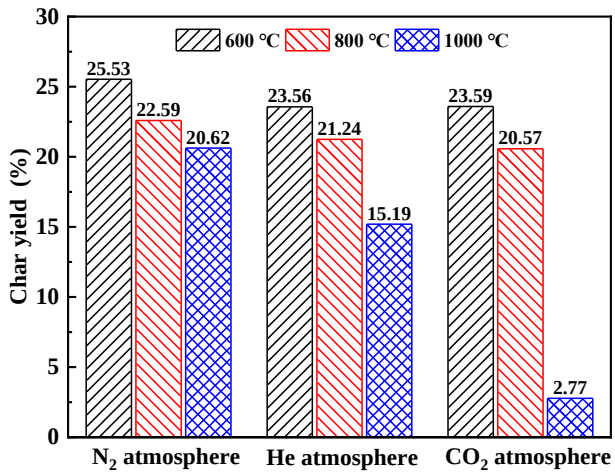

Fig. 1. Biochar yield

3.1.2 Pore structure analysis

The results of biochar surface morphology analysis are shown in Fig.2. It can be seen that with the change of biochar preparation temperature and atmosphere, the surface structures of biochar have different morphologies. Fig.2a-c shows the morphology of the biochar obtained under the N_2 atmosphere. From the Fig.2a, it can be found that volatile matter release during the heating process led to the creation of porosity in the biochar structure at 600 °C. With the biochar preparation temperature rising to 800 °C, the pore structure was developed with surface crack appeared, which results in the gradual destruction of surface structure (Fig.2b). Under a higher biochar preparation temperature (1000 °C), the excessive heat caused the biochar structure further fractured with more cracks appeared. The crystal cell structure was melting leading to the carbon skeleton gradually destroyed [18].

The SEM analysis of the biochar prepared in He atmosphere are shown in Fig.2d-f. The biochar prepared at 600 °C showed a rod-shaped structure with considerable cracks and small floccules on the external surface (Fig.2d). The pores further developed, and many new pores appeared on the surface at 800 °C (Fig.2e). While slight deformation and melting phenomenon were observed at 1000 °C, the biochar surface was still remained a tubular morphological skeleton structure (Fig. 2f). Comparing Fig. 2 c and f, it is found that the carbon skeleton of He-1000 was more complete than that of N_2-1000 under inert environment. During biomass devolatilisation in N_2 at 1000 °C, the particle first swelled and then melted, ruptured and loses its volatile matter [8]. However, the chemical properties of He is highly stable and act as a protective gas. During biomass devolatilisation in He, there was no expansion and fracture occurred, and this made the He-1000 having a complete rod-shaped structure.

Fig.2g-i present the morphology of the biochar prepared in CO_2 atmosphere. In Fig.2g, a gully and cavity structure were seen on the surface at 600 °C, indicating a gradually destruction of carbonaceous structure. Fig.2h shows the morphology of biochar at 800 °C, it can be seen that high temperature caused surface cracking deepened, with increased surface pores and roughness leading to collapses on the material surface. The CO_2 is reduced by carbon at high temperature (1000 °C). The consumption of carbon on the biochar particles structure resulted in balling phenomena and generation of sintering neck. Part of the particles were stuck together, which eventually destroyed the porous structure of the biochar (Fig.2i).

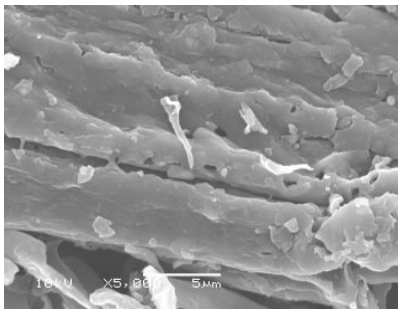

(a) N_2-600

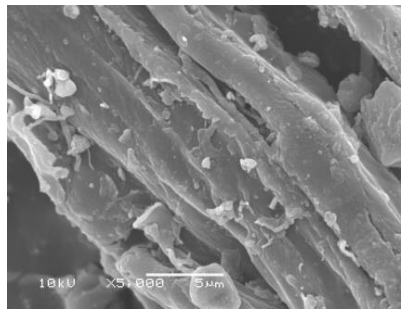

(b) N_2-800

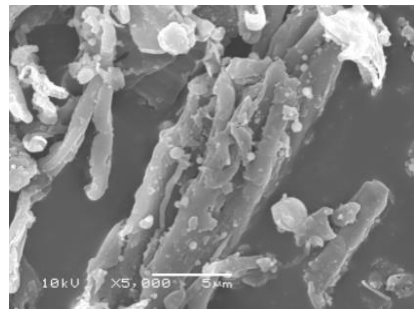

(c) N_2-1000

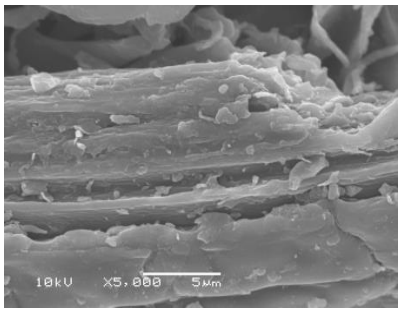

(d) He-600

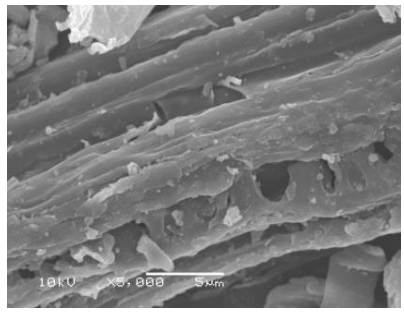

(e) He-800

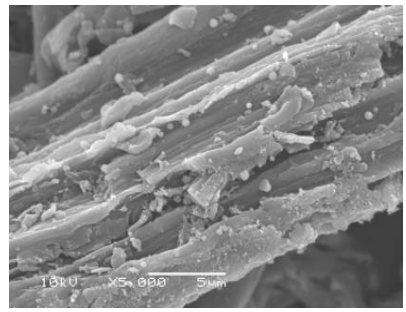

(f) He-1000

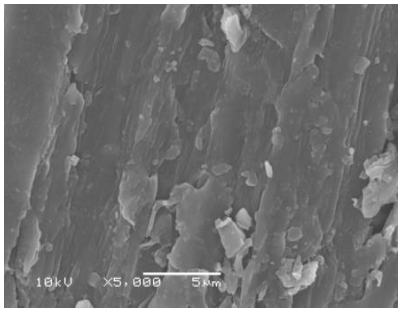

(g) CO_2-600

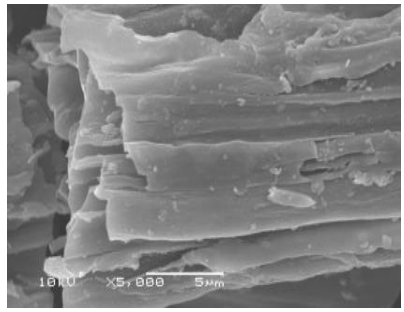

(h) CO_2-800

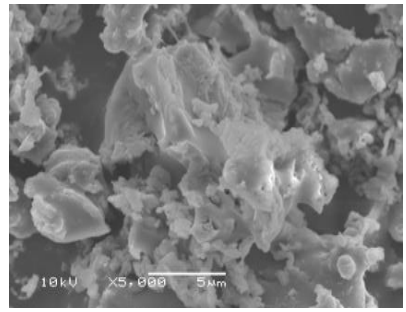

(i) CO_2-1000

Fig. 2. SEM images of biochar prepared at 600, 800, 1000 °C: (a)-(c) N_2 atmosphere, (d)-(f) He atmosphere and (g)-(i) CO_2 atmosphere.

Table 2 shows the relative content of mineral elements on the different biochar by EDX characterisation. It can be seen that evident differences in the concentration of individual elements were observed from different biochar. It was known that the alkali and alkali earth metal elements (AAEMs) in the biochar were the active catalyst. The AAEMs in biochar have a catalytic effect on the primary devolatilisation and secondary cracking, which can reduce the activation energy and increase the gas product yields. In addition, they can also play a noticeable role in inhibiting biochar graphitisation and vapor/tar condensation during the gasification process [18].

Furthermore, it can be observed from the parametric analysis that the increase of biochar preparation temperature, can increase the contents of Ca, Mg and K in the CO_2 biochar but reduce the contents of Ca and K in the N_2 biochar reduced. The trend of Ca, Mg and K content in the He biochar increased first and then decreased with the increase of preparation temperature. Inorganic elements present in the biomasses are responsible for ash content of the biochar [34]. Since CO_2-1000 contain relatively higher ash content, which made its mineral element content greatly different from that of other samples, it is not surprising to see that produced biochar contains significant amounts Si and other inorganics. During the pyrolysis of biomass (biochar production), K release amount increased significantly with the increase of biochar production temperature, and the K entered the gas phase as KCl and KOH at high-temperature, which made the content of K decreased in the N_2 biochar and He biochar. Due to the behaviour of Ca largely depends on their secondary transformations both inside and over biochar particles, some calcium compounds in the biochar was decomposed after melting and joined the volatile to become part of the vapor phase product at high temperature. This resulted in the content of Ca in the N_2 biochar and He biochar decreased [35]. However, under CO_2

atmosphere, K^+, Ca^{2+} combined with CO_2 to form solid products of K and Ca (such as K_2CO_3, $CaCO_3$), which made the content of K, Ca increased in the CO_2 biochar.

Table 2 Elemental analysis (by EDX)

Samples	Mg (wt.%)	Si (wt.%)	P (wt.%)	S (wt.%)	K (wt.%)	Ca (wt.%)
N_2-600	0.37	6.58	0.29	0.35	3.32	2.76
N_2-800	0.54	1.24	0.25	0.27	1.04	1.39
N_2-1000	0.39	0.77	0.18	1.05	1.16	0.66
He -600	0.32	2.83	0.32	0.18	1.67	1.08
He -800	0.86	2.74	0.48	0.29	2.44	2.72
He -1000	0.31	0.71	0.25	0.50	0.15	1.02
CO_2-600	0.37	1.14	0.19	0.12	0.76	0.44
CO_2-800	0.64	1.79	1.73	0.28	1.95	3.14
CO_2-1000	2.35	52.72	0.00	0.00	20.21	10.36

The results of N_2 adsorption isotherms of biochar are shown in Fig.3. It can be found that the volume of N_2 adsorbed increased noticeably (except CO_2-1000) at the relative pressure smaller than 0.1. This indicated that a strong interaction between biochar and nitrogen and proved that there has been abundant micropores existing. When the relative pressure continued to rise, the N_2 adsorption volume increased slowly, along with the simultaneous appearance of the hysteresis loop related to mesopore in biochar. It is noted that the hysteresis loops of 800 and 1000 °C were highly noticeable (except CO_2-1000) [36]. From Fig.3a-b, it can be found that the adsorption volume of the N_2 biochar and He biochar significantly increased with the biochar preparation temperature rising, which indicated the further development of the porous structure. However, it can be seen from Fig.3c that the biochar preparation temperature increased from 800 to 1000 °C, the adsorption volume of the CO_2 biochar dramatically decreased from 176.5 to 2.2 $cm^3\ g^{-1}$. The main reason was that CO_2 reacted with carbon in the biochar at high-temperature and caused elimination of carbon links. This eventually resulted in

the phenomenon of sintering and fragmentation (as shown in Fig. 2i), leading to the loss of adsorption capability for the CO_2-1000.

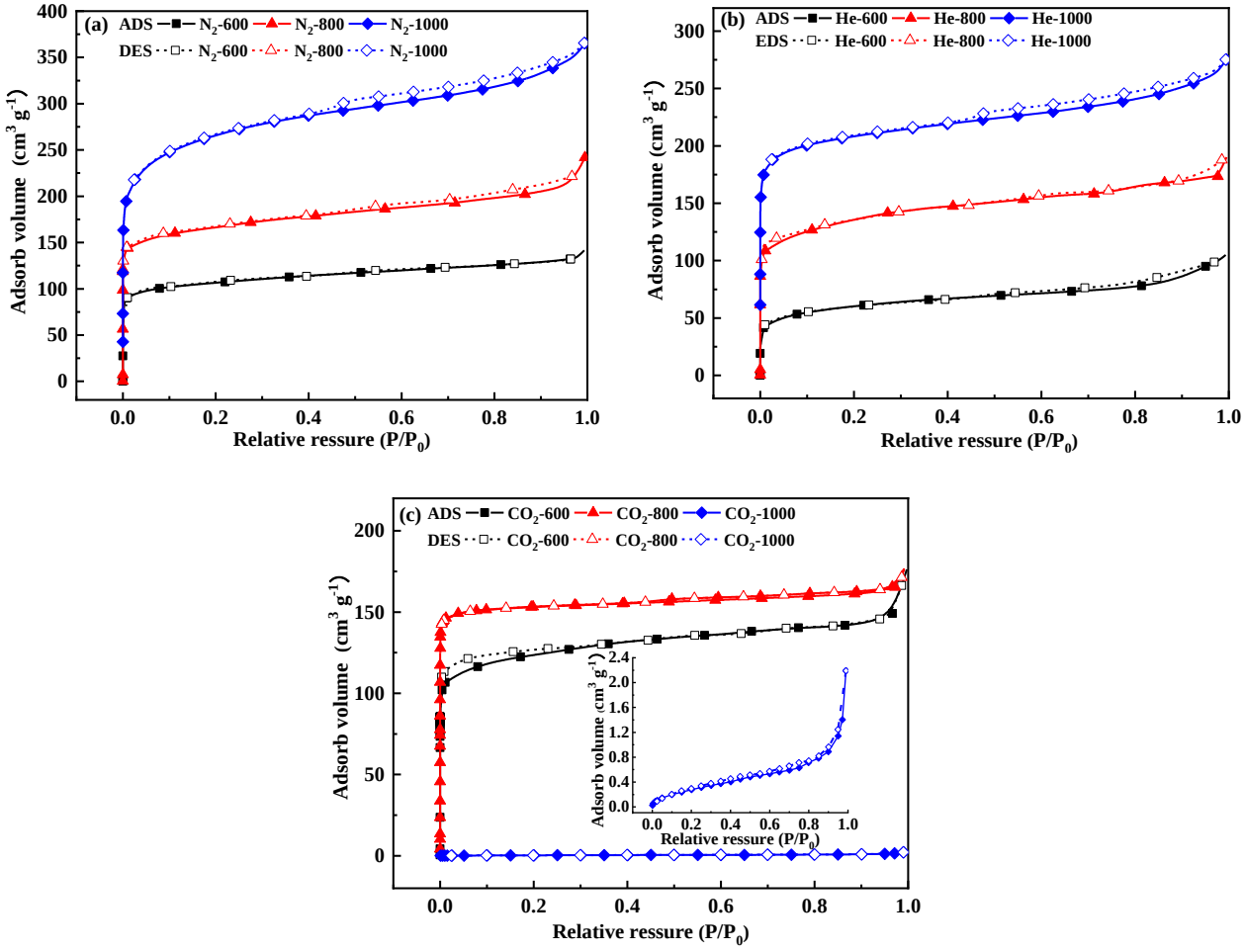

Fig.3 The N_2 adsorption-desorption isotherms for the biochar, produced under (a)N_2 atmosphere, (b)He atmosphere and (c) CO_2 atmosphere.

The pore size distribution of biochar illustrated in Fig.4. The results showed that the peak values of pore diameter change greatly with the pyrolysis conditions. All the pore size distribution curves (except CO_2-1000) appeared intensive peaks in the range of 0.25 - 1.5 nm and a small part of peaks between 2 and 4 nm, indicating the biochar contains a series of micropores (< 2 nm) and mesoporous (2-50 nm). The CO_2-1000 was found having a macrospore (> 50 nm) abundant structure (Fig.4c). It manifested that high preparation temperature and processing environment (CO_2) enlarged of pore size as well as the amounts of micro- and mesoporous [36].

Besides, it was worth noting that the number of micropores distribution of N_2 biochar and He biochar reached the maximum at 1000 °C, while that of the CO_2 biochar reached the maximum at 800 °C.

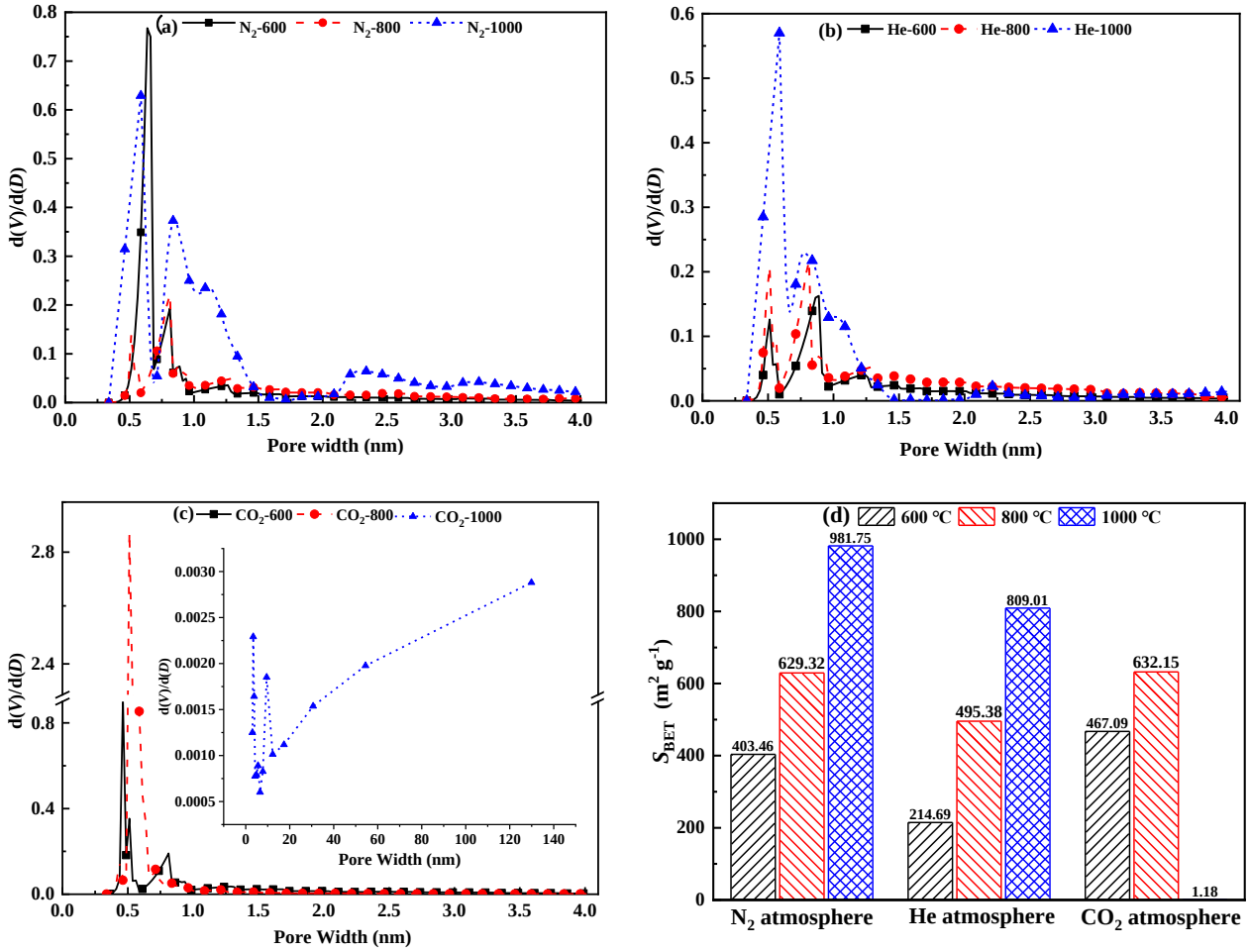

Fig.4 Pore size distribution of biochar prepared at 600, 800 and 1000 °C under (a)N_2 atmosphere, (b)He atmosphere and (c) CO_2 atmosphere. (d) BET Specific surface areas (S_{BET}) of biochar.

The specific surface area (S_{BET}) gave a quantitative comparison on the pore structure (shown in Fig 4d). As the biochar preparation temperature increased from 600 to 1000 °C, the S_{BET} of the N_2 biochar increased from 403.46 to 981.75 m^2 g^{-1}, while the S_{BET} of He char increased from 214.69 to 809.01 m^2 g^{-1}. This confirmed that the release of volatile could enhance the pore structure at higher biochar preparation temperature. For CO_2 biochar, the S_{BET} firstly increased but eventually vanished. The S_{BET} of the CO_2 biochar decreased from 632.15 to 1.18 m^2 g^{-1} when the temperature increased from 800 to 1000 °C. The neck formation and melting

phenomenon of CO_2-1000 resulted in the value of S_{BET} losing the specific area. Also as shown in Table 1, the CO_2-1000 contains almost ash (76.95%), meaning the lack of enough carbon to maintain the porous framework. The order of S_{BET} sequence for biochar under the same biochar preparation temperature (600 and 800 °C) can be ranked as CO_2 biochar > N_2 biochar > He biochar. With the carbon reduction effect, CO_2 is the most effective medium to create high S_{BET} among the three gases.

3.1.3 X-ray diffraction analysis

The XRD analysis on the graphitised crystal structure was shown in Fig.5. Two obvious diffraction peaks in the XRD curve the peak at 22° (002 peak) was related to stacking in aromatic layers and the peak at 47° (100 peak) represented the distance between points in an aromatic layer. The peak at about 15-22° is a γ band, which is caused by the aliphatic side chains, condensed saturated rings, or the adjacent chains of linear polymer [37, 38]. As can be seen from Fig.5a-b, with biochar preparation temperature increased from 600 to 1000 °C, the (002) peak of N_2 biochar and He biochar were noticeably enhanced (becoming taller and slimmer). This meant high temperature enhance the degree of aromatisation in carbon structure [18]. In Fig. 5c it can be seen that the position of the (002) peak shifted from 22° to 28° with the increase of biochar preparation temperature, close to that of graphite (26.6°), which indicated the structure was becoming more graphitic [37]. In addition, at 1000 °C, it can be found that the (002) peak intensity of biochar are N_2, He and CO_2 from high to small. This indicated the order of the aromatisation degree of biochar obtained under three atmospheres. In addition, the (100) peak for the N_2 char became sharper with the increase of biochar preparation temperature, indicating that high temperature enhances the degree of carbon ordering. It can be found from Fig.5b that the change of (100) peaks for He char was minor. In the Fig. 5c, it is worth noting that the (100) peak of CO_2 has gone flatten at 1000 °C.

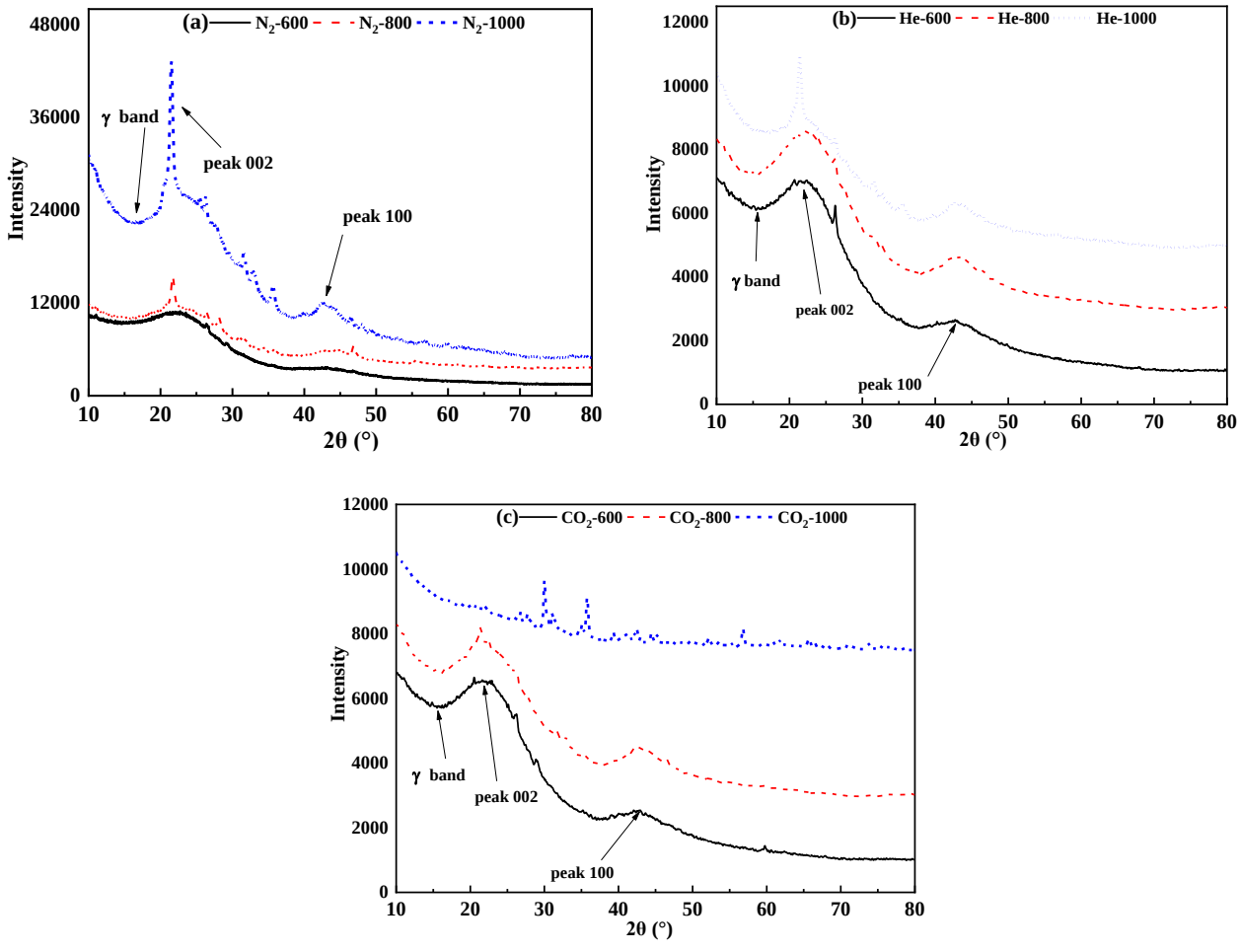

Fig.5. The X-ray diffraction patterns of biochar prepared at 600, 800 and 1000 °C under (a) N_2 atmosphere, (b) He atmosphere and (c) CO_2 atmosphere.

The structural parameters such as interlayer spacing d_{002} and crystallite height L_c were calculated by Bragg and Scherer equations. The d_{002} represents the degree of perfection in the periodicity of the stacking structure of aromatic layers and an estimation of the graphitisation degree of carbon; while the *L*c relates to the change of crystallite size in-plane and the coalescence of crystallites along the c-axis [37]. The high d_{002} and low *L*c values meant that poorer crystallinity or a lower degree of graphitisation in the studied biochar samples [38, 39]. It was found from the crystal structure parameters (Table.3) that the crystallinity index CrI of biochar increased with the biochar preparation temperature increasing. A high CrI value meant a high degree of graphitisation [18]. It also can be seen that the highest CrI value was N_2 biochar, while the lowest was CO_2

biochar. In addition, with the biochar preparation temperature increased from 600 to 1000 °C, the value of interlayer spacing d_{002} decreased, while the crystallite height L_c increased. This meant that the aromatic layer became closer and sturdier, and the order of the microcrystalline arrangement become more consistent, which implied a good degree of graphitisation [7]. The increase of CrI and L_c values indicated the biochar produced under a high temperature tends to have high degree of graphitisation, which gives a potential lower gasification reactivity.

Table 3 Microcrystalline parameters

Samples	CrI	d_{002} (nm)	L_C (nm)
N_2-600	0.64	0.4138	0.37
N_2-800	0.75	0.4113	0.41
N_2-1000	0.77	0.4050	0.54
He-600	0.64	0.4193	0.30
He -800	0.68	0.4155	0.32
He -1000	0.74	0.4145	0.33
CO_2-600	0.64	0.4192	0.41
CO_2-800	0.67	0.4006	0.56
CO_2-1000	0.69	0.4091	1.39

3.2 Gasification characteristics of biochar

3.2.1 Isothermal gasification reactivity analysis

The CO_2 gasification reactivity of the biochar is shown in Fig.6. Under the same gasification temperature, the normalised gasification rate K values (Eq.3) of N_2 biochar and He biochar deceased with the raise of biochar preparation temperature. The low K value meant a relatively low gasification reactivity, which is in line with the conclusion drawn in Section 3.1.3. For CO_2 biochar, the tendency of K values was same to those of N_2 biochar and He biochar when the gasification temperature was 800 °C. However, when the gasification temperature was higher than 800 °C, the K values of CO_2 biochar fluctuated with the biochar preparation

temperature increasing. The main reason of this phenomena is that the reaction between C and CO_2 is an endothermic reaction, high gasification temperature can promote the gasification process. The CO_2-800 has a high S_{BET} of 632.15 m^2 g^{-1} with high contents of AAEMs, which enable the biochar having a high gasification reactivity. The CO_2-1000 was mainly composed of ash (76.95%) with a very low fixed carbon content (23.05%) which limited the CO_2 reduction reaction. For the biochar prepared under the same heating temperature, it can be observed that the atmosphere has an influence on the gasification reactivity of char. The order of the *K* values for the biochar prepared at 600 and 1000 °C was He biochar > N_2 biochar > CO_2 biochar, indicating that the He biochar had the best gasification reactivity, followed by N_2 biochar and CO_2 biochar. The ordering the *K* values of biochar prepared at 800 °C form high to low is CO_2 biochar, He biochar and N_2 biochar.

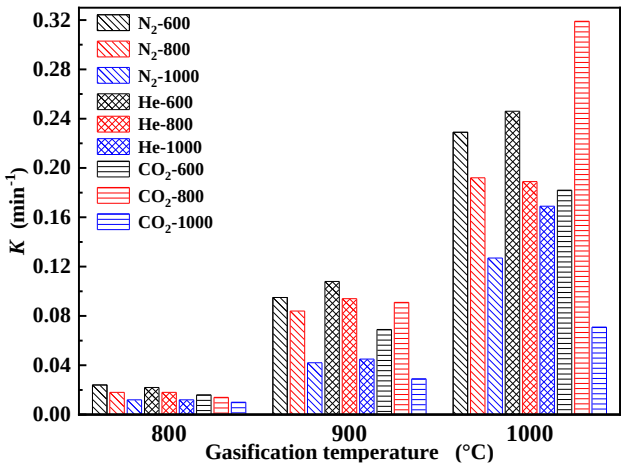

Fig.6 Comparison of normalised gasification rate *K*

Correlating the finding from Fig.4d and Fig 6, it is inferred that the level of specific surface area matched the order of gasification reactivity of CO_2 biochar. The S_{BET} and gasification reactivity of CO_2 biochar first increased and then reduced with the biochar preparation temperature rising. However, the variation of AAEMs content and microcrystalline structure was not consistent with the gasification characteristics. It can be inferred

that the S_{BET} is the dominating factor for the gasification reactivity of CO_2 biochar. This is in an agreement with Malekshahian et al [40] that the pore structure of biochar was a decisive factor for its gasification reactivity.

The gasification temperature has a remarkable influence on the gasification reactivity. It can be seen from Fig.6 that, when the gasification temperature increased from 800 to 1000 °C, the *K* values were greatly increased. This indicated that the high gasification temperature could result in a better reactivity. When the gasification temperature rose from 800 to 1000 °C, the gasification reactivity of biochar increased by 9.5-22.8 times. However, the change of biochar preparation temperature only resulted in 1.1-2.4 times increase on the reactivity. Changing the processing atmosphere can only increase the reactivity by 1.1-2.3 times. This indicated that the gasification temperature had a greatest impact on the CO_2 gasification reactivity, followed by biochar preparation temperature, and processing atmosphere was the lowest.

3.2.2 Non-isothermal gasification reactivity analysis

The results of non-isothermal carbon conversion rate (Eq.1) and gasification rate (Eq.2) for biochar are shown in Fig.7. When gasification temperature exceeded 600 °C, the gasification rate started to increase gradually and reach a single peak of gasification rate. The carbon conversion rate presented a three-stage curve. The temperature was less than T_i in the first stage, the weight loss remained unchanged. When the temperature increased from T_i to T_f, the biochar continually devolatilised and reacted with the CO_2 to produce syngas. The final stage was the end of gasification process with most of carbon converted and ash remained as a residue.

Since the main gasification process occurred at the second stage, the focus of the kinetics study was concentrated on the this stage for the best representation of the gasification process [3]. In order to enhance the accuracy of the analysis, the gasification characteristic parameters T_i, T_m, T_f and S (Eq.4) were used to represent

gasification reactivity of biochar. The results are shown in Table 4. Under the same heating rate and processing atmosphere, when the biochar preparation temperature increased from 600 to 1000 °C, the values of T_i, T_m and T_f of N_2 biochar and He biochar all increased, but the S values of those decreased. High T_m and T_f values and lower S value indicated the a low gasification reactivity [3, 6]. This meant that high biochar preparation temperature could result in decreased gasification reactivity. For the CO_2 biochar, the increase of biochar preparation temperature also reduced the values of T_i, T_m and T_f, while the values of S and dx/dt_{max} increased first and decreased. Based on Eq (4), it can be derived that the value of S will increase when the gasification rate (dx/dt_{max} and dx/dt_{mean}) and gasification temperature (T_i and T_f) rise simultaneously. This indicated that the effect of reaction rate was stronger than that of the temperature for gasification process. This is in agreement with the results from Tong et al [7]. At the same time, it is found from the change of S values in Table 4, when the heating rate rose from 5 to 20 °C min^{-1}, the gasification reactivity of biochar increased by 1.9-7.6 times. However, the change of biochar preparation temperature and the processing atmosphere all resulted in 0.1-0.9 times increase on the reactivity. This indicated that the heating rate had the greatest impact on the gasification reactivity, followed by biochar preparation temperature and processing atmosphere. The S values of biochar prepared at 600 and 1000 °C were in the order of He biochar > N_2 biochar > CO_2 biochar, indicating that producing biochar under the He atmosphere gave the highest gasification reactivity, while under CO_2 give the lowest. For the biochar prepared at 800 °C, CO_2 atmosphere gave highest gasification reactivity.

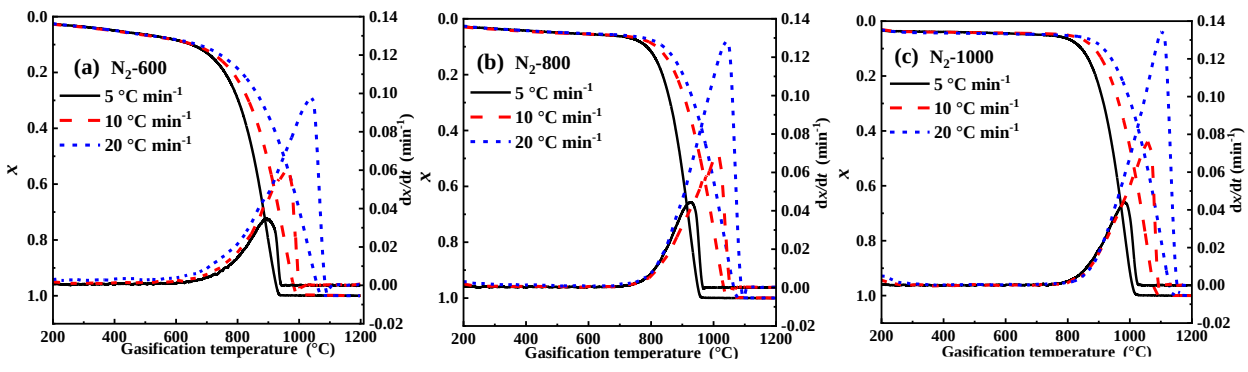

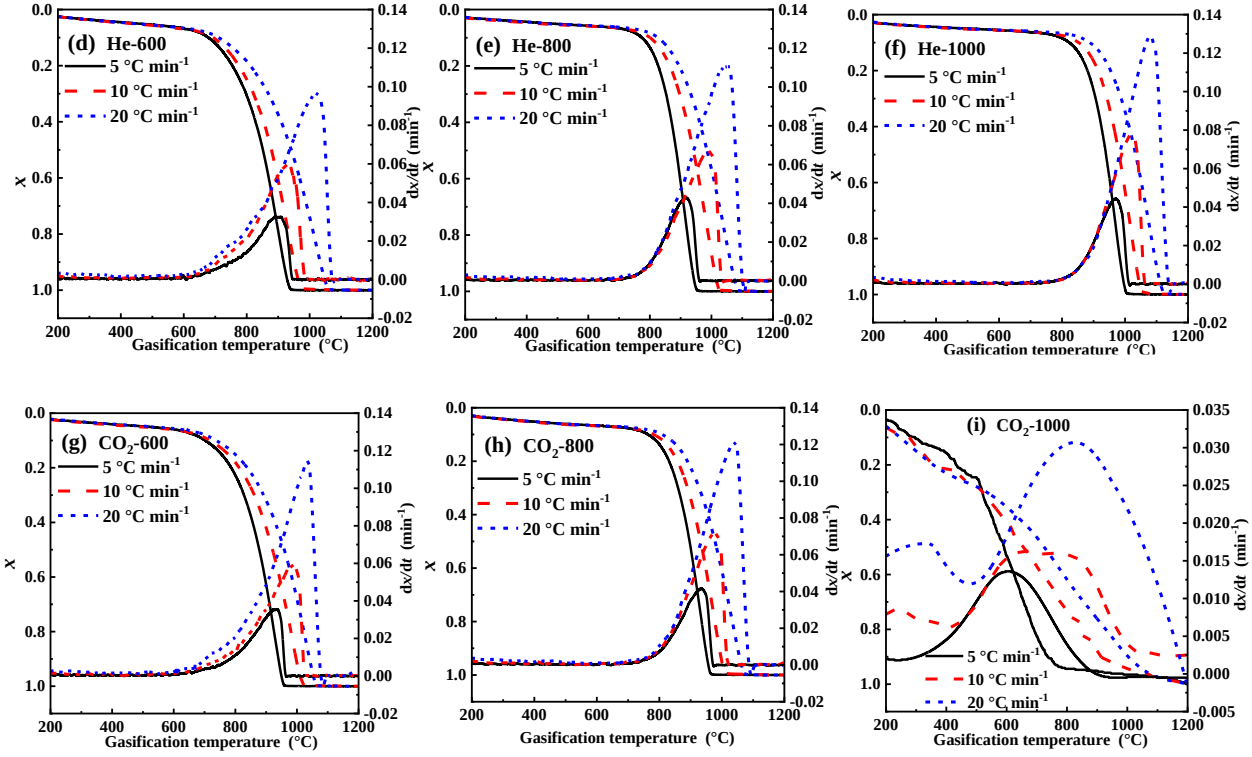

Fig. 7 The carbon conversion rate and gasification rate curves of biochar prepared at 600, 800 and 1000 °C under (a)-(c) N_2 atmosphere, (d)-(f) He atmosphere and (g)-(i) CO_2 atmosphere.

Table 4 Gasification reactivity parameters under different heating rates

Samples	β (°C min^{-1})	T_i (°C)	T_m (°C)	T_f (°C)	dx/dt_{max} (min^{-1})	dx/dt_{mean} (min^{-1})	S (10^{-13})	M_{ash}* (%)
N_2-600	5	635	894	945	0.0350	0.0044	4.04	11.91
	10	690	960	1006	0.0592	0.0086	10.63	11.58
	20	701	1042	1093	0.0978	0.0168	30.59	12.07
N_2-800	5	736	926	980	0.0445	0.0044	3.69	11.69
	10	760	1013	1050	0.0691	0.0081	9.23	11.76
	20	830	1044	1130	0.1282	0.0168	27..67	12.42
N_2-1000	5	743	984	1037	0.0439	0.0044	3.37	14.42
	10	794	1059	1104	0.0761	0.0086	9.41	22.08
	20	855	1101	1175	0.1344	0.0168	26.29	14.35
He-600	5	610	890	941	0.0328	0.0044	4.12	12.01
	10	635	933	987	0.0601	0.0085	12.83	11.22
	20	657	1019	1068	0.0970	0.0168	35.35	11.90
He-800	5	703	917	971	0.0431	0.0044	3.95	13.35

	10	740	991	1042	0.0671	0.0087	10.23	12.62
	20	789	1047	1080	0.1116	0.0169	28.05	13.27
	5	724	971	1027	0.0446	0.0044	3.65	16.13
He-1000	10	785	1023	1090	0.0780	0.0086	9.90	15.66
	20	825	1081	1147	0.1291	0.0168	27.78	16.49
	5	652	933	976	0.0357	0.0044	3.79	11.62
CO_2-600	10	705	986	1023	0.0595	0.0086	10.06	10.88
	20	740	1035	1098	0.1148	0.0170	32.46	11.58
	5	690	934	968	0.0417	0.0044	3.98	17.52
CO_2-800	10	706	978	1017	0.0722	0.0086	12.25	17.02
	20	751	1043	1086	0.1214	0.0168	33.30	17.61
	5	353	596	974	0.0136	0.0046	5.15	96.38
CO_2-1000	10	408	653	1038	0.0163	0.0091	8.58	95.50
	20	534	823	1105	0.0307	0.0151	14.71	95.05

* M_{ash} denotes the mass of ash residue after the gasification run.

Table 4 and Fig 7 also presented that the heating rates had a noticeable impact on the gasification reactivity. It was clear that the curves for carbon conversion rate and gasification rate moved towards the high-temperature region with the increase of the heating rate. It can be found from Fig.7 that with the heating rate increasing, the value of carbon conversion rate reduced, while the gasification rate increased. This was because that, under the high heating rate, the biochar did not have enough time to complete the reaction [18]. Together with the thermal hysteresis effect [3, 6], high heating rate resulted in low carbon conversion rate. Nevertheless, it can be seen from Table 4 that heating rate caused gradual increased dx/dt_{max}, dx/dt_{mean} and S values, which indicated that high heating rate could improve the gasification reactivity. Taking N_2-600 as an example, with heating rate increased from 5 to 20 °C min^{-1}, index S increased from 4.04×10^{-13} to 3.06×10^{-12}. In addition, it can be observed that the values of T_i, T_m and T_f increased with the heating rate increased from 5 to 20°C min^{-1}, and the effect of increasing heating rate on the T_i was much smaller than that of T_m and T_f (taking He-600 as the example that the difference of T_i, T_m and T_f were 47, 129 and 127 °C, respectively). At the early stage of gasification, due to

the low gasification temperature and slow reaction speed, the effect of reaction temperature superposition and lag was limited. With the gasification reaction going on, the carbon in biochar is gradually consumed. The influence of heat transfer is reduced, and the superposition effect is more obvious. At the end of the gasification, the temperature difference between the inner and surface of the sample is eliminated. The superposition effect of the gasification reaction is the main reason for a high T_m and T_f when the heating rate is high [6].

3.3 Gasification kinetic analysis

3.3.1 Isothermal gasification kinetic analysis

The HM model (Eq.5) is the most used model to describe biochar CO_2 gasification, and the kinetic results for various biochar listed in Table 5. For N_2 biochar and He biochar, it can be seen that the *E* and *A* by the HM model increased when biochar preparation temperature was increased. The high *E* value meant that the CO_2 gasification reaction of biochar was hard to proceed, which was consistent with the results of XRD analysis. Generally, the value of *E* increased with the increase of biochar preparation temperature. However, it can be found from Table 5 that the *E* values of CO_2-1000 char was 78.09 kJ mol^{-1}, which was much smaller than those of biochar at 600 and 800 °C. This is because the CO_2-1000 char contained a high amount of AAEMs (Table 2), such as K (20.21%), Ca (10.36%), Mg (2.35%). Lahijani et al. [41] investigated the influence of AAEMs on the CO_2 gasification reactivity of pistachio nutshell char. It was found that the *E* value of biochar loaded with AAEMs was 53 kJ mol^{-1} lower than that of uncatalysed biochar. The correlation coefficient R^2 reached above 0.95, meaning that the HM model had a good fitting effect. In this study, the values of *E* for N_2 biochar were in the range of 119.90-204.86 kJ mol^{-1}, He biochar 123.44-212.46 kJ mol^{-1} and CO_2 biochar 78.09-183.88 kJ mol^{-1}. The values of *E* for biochar obtained under various processing conditions were close, mainly in the range of 78.09 - 212.46 kJ mol^{-1}. This was consistent with the results from Blasi et al. [42] that the *E* values of

biochar gasification varied in the range of 80.3-261 kJ mol^{-1}. Wang et al. [6] calculated the *E* values of CO_2 gasification of corncob biochar prepared at N_2, CO, He and CO_2 atmosphere was in the range of 221-258.1 kJ mol^{-1}. Comparing to the previous works, it can see that the value of *E* obtained in this study are in the normal range. Furthermore, according to the studied of above gasification reactivity that the *E* of CO_2-800 was 183.9 kJ mol^{-1}, which was obviously higher than those of He-800 and N_2-800. Similar results were also reported by Li et al [3] and Wang et al [6] that high gasification reactivity resulted in high of the activation energy of the reaction system. When the biochar preparation temperature raised from 800 to 1000 °C, the *E* increased by 70 kJ mol^{-1} for N_2 biochar and He biochar. This was about five times higher than the increase of the *E* when the biochar preparation temperature raised from 600 to 800 °C. This indicated that biochar produced at high temperatures has a better heat resistance and requires more energy to be converted. Meanwhile, CO_2 can react with carbon in biochar at high-temperature and this result in low biochar yield with a relatively poor pore structure. In the real industrial application, the biochar produced at high temperature may have relatively a low quality.

According the results shown in Table 5, the change trend of *E* was consistent with that of *A* for the biochar prepared at N_2, He and CO_2 atmosphere under different temperatures. In addition, it is found from Table 5 that the *E* values and the *A* change in the same direction, which is referred to as the compensation effect [6]. The kinetic compensation effect is said to occur when there is a linear relationship between ln*A* and *E* ($\ln A = aE + b$) for a gasification reaction processes. The R^2 values were all greater than 0.99, this indicated an obvious kinetic compensation effect in the CO_2 gasification process of biochar in this study. According to the study by K. Yip et al.[43] , the selective oxidation of carbon materials with heterogeneous carbon structures was the key factor determining the kinetic compensation effect.

Table 5 Calculated kinetic parameters

Samples	E (kJ mol^{-1})	A (min^{-1})	R^2	ln$A$=aE+b
N_2-600	119.90	11916	0.9961	ln$A$=0.09E-1.20 R^2=0.9999
N_2-800	137.73	54583	0.9594	
N_2-1000	204.86	21001407	0.9915	
He-600	123.44	17727	0.9727	ln$A$=0.09E-1.49 R^2=0.9992
He-800	137.85	58431	0.9978	
He-1000	212.46	57297067	0.9936	
CO_2-600	127.36	17535	0.9787	ln$A$=0.09E-1.14 R^2=0.9954
CO_2-800	183.88	8153028	0.9639	
CO_2-1000	78.09	330	0.9946	

3.3.2 Non-isothermal gasification kinetic analysis

The FWO method (Eq.7) was employed to study the kinetics of biochar CO_2 gasification at various heating rates. The calculated E values at x= 0.1-0.9 were analysed. The results of lnβ against 1000/T fitting straight line are shown in Fig.8. It is clear that the trend of changes in the fitting line gained from the FWO model at different carbon conversion rates were consistent. The results from the approximate parallel regression indicated that the E determined at different carbon conversion rates can be described by a one-step reaction mechanism or a unity of multiple reaction mechanisms. In addition, as shown in Fig.8 the R^2 can prove the results of calculated E values were sufficiently accurate and reliable.

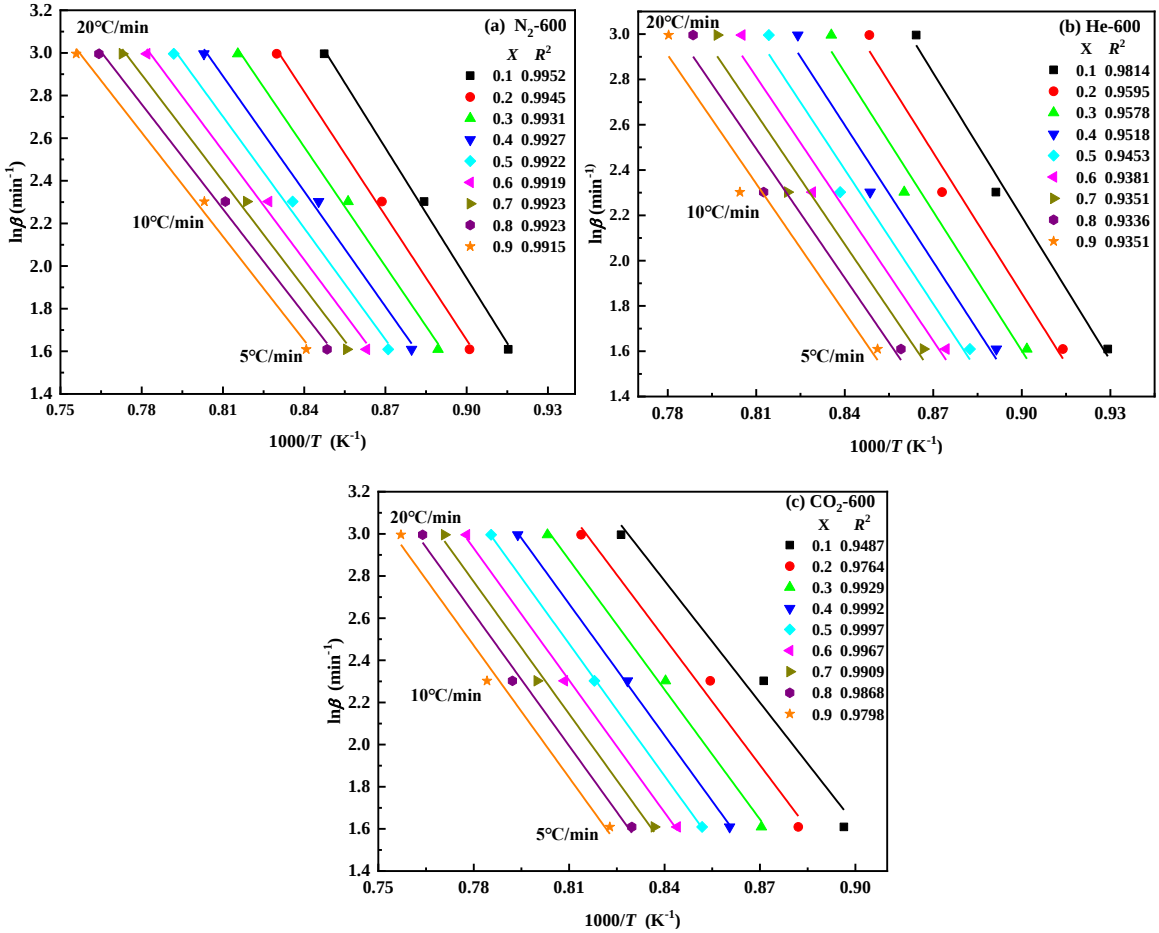

Fig. 8 Linear relationship between lnβ and 1000/T of biochar of produced under (a) N_2 atmosphere, (b) He atmosphere and (c) CO_2 atmosphere at 600 °C

As shown in Fig. 9, the E values decreased with increasing carbon conversion x (except CO_2-600), which indicated that the higher conversion was favourable for gasification reaction. At the early stage of gasification reaction (x= 0.1-0.2), it was considered that the biochar was difficult to react as a result of low volatility and insufficient temperature. The E decreased quickly in the range of x= 0.3-0.7 and reduced slowly x= 0.8-0.9. As the gasification temperature increased, the biochar reacted with the CO_2 enough reaction and required less energy to stabilise the gasification process. At the later stage of the gasification reaction, the carbon in biochar reacts completely with CO_2, the heat transfer effect was reduced, and the process required less energy to maintain the gasification reaction. The average value of activation energy E_a raised with the biochar preparation

temperature increasing. High value of E_a indicated that the gasification reaction required more energy and time to proceed. The low E_a of CO_2-1000 was due to its rich AAEMs. The E_a of biochar obtained from N_2, He and CO_2 atmosphere calculated by the FWO method was 148-175, 155-190 and 65-196 kJ mol^{-1}, respectively. The calculated E_a values with great accuracy can be applied in the master curve method to determine the mechanism function $f(x)$.

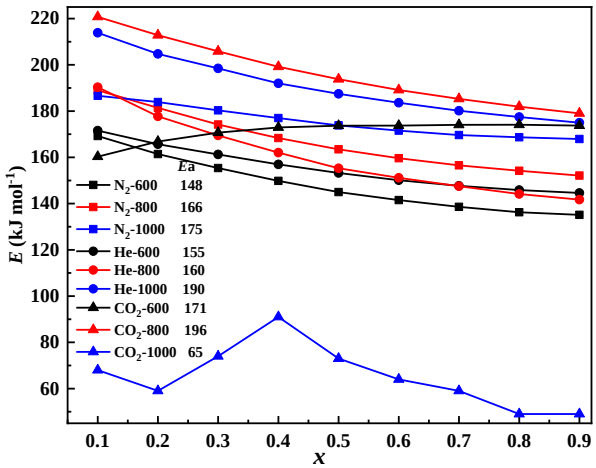

Fig. 9 Correlation between E and x.

3.3.3 Determination of mechanism function *f*(x)

The E, A and $f(x)$ for the gasification of biochar obtained from three biochar preparation temperatures were calculated to describe the non-isothermal gasification reaction process of biochar prepared at N_2, He and CO_2 atmospheres. According to Eq.10, the theoretical master plots of $G(x)/G(x_{0.5})$ versus x and experimental master plots of $P(u)/P(u_{0.5})$ versus x were obtained. As shown in Fig.10 a-c, the experimental master plots from the gasification of biochar were compared with the theoretical master plots. When the carbon conversion rate was 0.1-0.9, it can be observed that the plots of $P(u)/P(u_{0.5})$ versus x from the gasification of biochar at different biochar preparation temperatures were in a similar change trend, but did not completely coincide with

any theoretical curve. The plots of $P(u)/P(u_{0.5})$ versus x from the gasification of N_2 biochar consistent with the theoretical master plot A3, as shown in Fig.10a, considered its gasification kinetics conformed to the reaction mechanism of three-dimensional random nucleation and nuclei growth. With respect to the He biochar, it can be found from Fig.10b that the plots of $P(u)/P(u_{0.5})$ versus x were located between the theoretical master plots R1 and A2, this showed that the He biochar gasification kinetics conformed to the reaction mechanism of random nucleation and phase boundary. From Fig.10c, the experimental curve of CO_2 biochar did not completely coincide with any theoretical curve, it can be seen that the biochar prepared at 600 and 800 °C, the plots of $P(u)/P(u_{0.5})$ versus x were coincided with the theoretical master plot R1. When the biochar preparation temperature reached 1000 °C, the results showed that D3 mechanism was applicable to the early stage (x < 0.5) of the CO_2-1000 gasification process and F3 mechanism at later stage (x > 0.5). It can be confirmed that the one-dimension phase boundary reaction mechanism was applicable to the gasification of CO_2 biochar prepared at lower temperature, and the three-way transport diffusion and third-order reaction mechanism at higher biochar preparation temperature. Due to the CO_2 can react with carbon and it caused the microstructure of biochar changed greatly in the pyrolysis process, so it cannot be described by a single reaction mechanism.

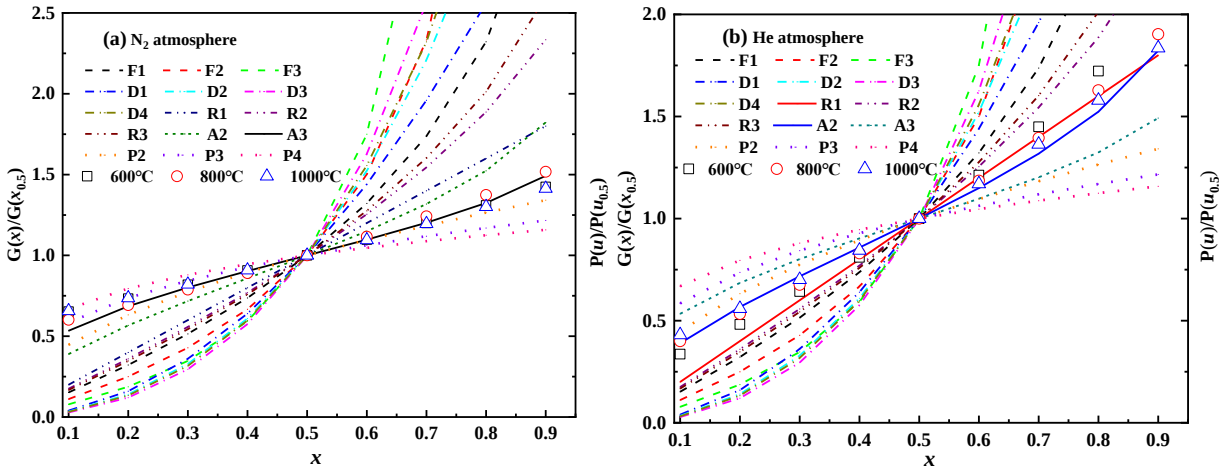

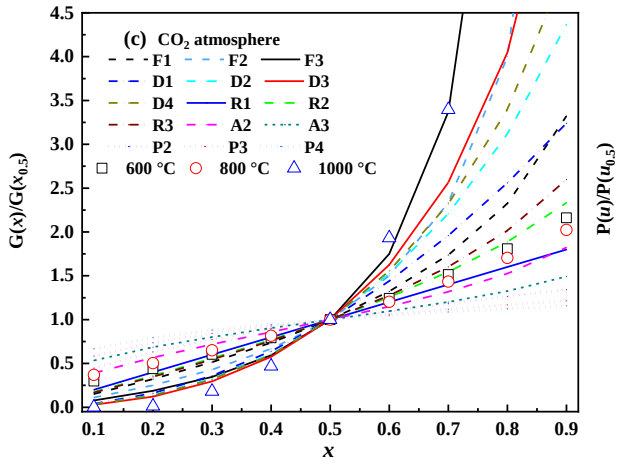

Fig.10 Experimental master-plots of $P(u)/P(u_{0.5})$ versus x from gasification of char produced under (a) N_2 atmosphere, (b) He atmosphere and (c) CO_2 atmosphere at 600,800 and 1000 °C and theoretical master-plots $G(x)/G(x_{0.5})$ versus x at 10 °C min^{-1}.

According to the above mechanism functions analysis, the $G(x)$ model was applied to determine the A. With the $G(x)$ model function substituted into the Eq.8 with performing the least-squares fit on $G(x)\sim[EP(u)/\beta R]$, the slope value A can be derived. The results of kinetic parameters are shown in Table 6. Various linear curve fits were plotted for ln A versus E_a and the results are shown in Fig. 11. The A and E_a fitted well to the equation of kinetic compensation effects ($\ln A = aE + b$). The fitting curves all had high correlation coefficients ($R^2 > 0.98$). These results indicated that the non-isothermal gasification of biochar presented an excellent dynamic compensation phenomenon. This also proved the applicability of the kinetic model in Table 6 for describing the reaction process of biochar non-isothermal gasification [31]. From this analysis, it can be inferred that these key kinetic parameters could provide critical theoretical basis for the research of non-isothermal gasification of biochar under CO_2 atmosphere.

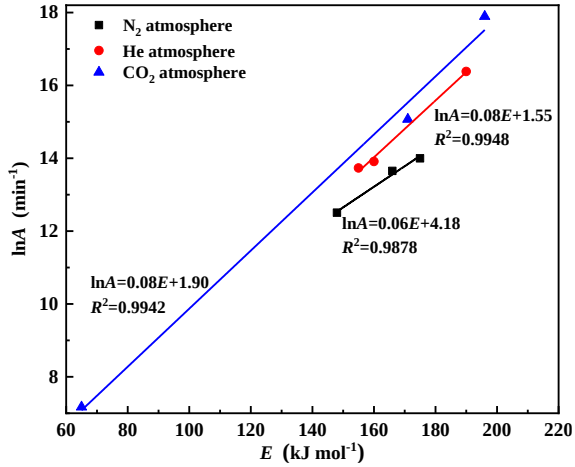

Fig.11 Kinetic analysis of non-isothermal gasification of biochar relationship between ln(*A*) and *E*.

Table 6 Kinetic triplets of the CO_2 gasification of biochar

Samples	*E* (kJ mol^{-1})	*A* (min^{-1})	R^2	*G*(*x*)	*f* (*x*)
N_2-600	148	2.7×10^5	0.9494		
N_2-800	166	8.5×10^5	0.9576	$[-\ln(1-x)]^{1/3}$	$3(1-x)[-\ln(1-x)]^{2/3}$
N_2-1000	175	1.2×10^6	0.9742		
He-600	155	9.2×10^5	0.9431		
He-800	160	1.1×10^6	0.9638	$x[-\ln(1-x)]^{1/2}$	$2(1-x)[-\ln(1-x)]^{1/2}$
He-1000	190	1.3×10^7	0.9682		
CO_2-600	171	3.5×10^6	0.9577		
CO_2-800	196	5.9×10^7	0.9715	x	1
CO_2-1000	65	1.3×10^3	0.9882	$[1-(1-x)^{1/3}]^2$ $x<0.5$; $[(1-x)-2]/2$ $x>0.5$	$1.5(1-x)^{2/3}[1-(1-x)^{1/3}]-1$ $x<0.5$; $(1-x)^3$ $x>0.5$

5. Conclusions

The effects of varying processing conditions on the physicochemical characteristics and gasification reactivity of biochar were studied. A comprehensive analysis was performed to correlate the composition and microstructure of biochar to the reactivity of biochar CO_2 gasification. The key findings are:

(1) With the increase of biochar preparation temperature, the biochar surface gradually diminished, and the pore structure developed with the microcrystalline becoming orderly and regularised. Under the same biochar preparation temperature, the S_{BET} for the biochar were in the order of CO_2 biochar > N_2 biochar > He biochar, and the ordering degree of biochar was in the order of N_2 biochar > He biochar > CO_2 biochar.

(2) The CO_2 gasification reactivities of the N_2 biochar and He biochar mostly depended on the microcrystalline structure. The gasification reactivity of N_2 biochar was also affected by the inherent ash metals. The specific surface area was the major factor on the gasification reactivity of CO_2 biochar.

(3) The gasification reactivities of N_2 biochar and He biochar were found decrease with the increase of biochar preparation temperature, while the CO_2 biochar prepared at 800 °C presented the highest gasification reactivity. For processing atmospheres, the reactivity of char prepared at 600 and 1000 °C was in the order of He biochar > N_2 biochar > CO_2 biochar, while the biochar reactivity prepared at 800 °C were CO_2 biochar > He biochar > N_2 biochar.

(4) The gasification reactivity increased with the increase of gasification temperature, while increasing the heating rate also stimulated the reaction. The influence of gasification temperature and heating rate on the gasification reactivities were greater than those of biochar preparation temperature and processing atmosphere.

(5) Kinetic analysis showed that the *E* values increased with the increase of biochar preparation temperature and decreased with the increase of carbon conversion rates. The master-plots method proved that the A3 mechanism was suitable for describing the gasification of N_2 biochar and the R1 and A2 mechanism were suitable to the He biochar gasification process. The R1 mechanism was appropriate to describe the

gasification of CO_2 biochar at lower biochar preparation temperature, and the D3 and F3 mechanism were applicable at high biochar preparation temperature.

ACKNOWLEDGEMENT

This work was supported by the Natural Science Foundation of China (No.51706022), the Natural Science Foundation of Hunan Province of China (No.2018JJ3545), Open Fund of Key Laboratory of Renewable Energy Electric-Technology of Hunan Province (No.2017ZNDL007), 2019 Graduate Research and Innovation Project at CSUST (No. CX2019SS22) and the Innovative Team of Key Technologies of Energy Conservation, Emission Reduction and Intelligent Control for Power-Generating Equipment and System at CSUST. The authors also would like to acknowledge the funding from EU Horizon 2020 Research and Innovation Program under the Marie Skłodowska-Curie Action (Grant Agreement No. 823745).

NOMENCLATURES

A	Pre-exponential factor
CrI	Crystallinity index
$\mathrm{d}x/\mathrm{d}t_{max}$	Maximum gasification reaction rate
$\mathrm{d}x/\mathrm{d}t_{mean}$	Mean gasification reaction rate
d_{002}	Interlayer spacing
E	Activation energy
$f(x)$	Mechanism function
$G(x)$	Integral form of reaction mechanism function
K	Normalised gasification rate
L_c	Crystallite height

$P(u)$	Temperature integral
r	Gasification rate
S	Gasification characteristic index
S_{BET}	Specific surface area
t	Gasification time
T_i	Initial reaction temperature
T_m	Temperature for peak conversion rate
T_f	Final reaction temperature
x	Carbon conversion rate

ABBREVIATIONS

AAEM	Alkali and alkaline earth metal
FWO	Flunm-Wall-Ozawa
HM	Hybrid model

RESEARCH DATA

The full research data for this paper is available at the Aston University's research repository. File link: http://researchdata.aston.ac.uk/471/

References

[1] Brosse N,Dufour A,Meng X ,et al.Miscanthus: a fast-growing crop for biofuels and chemicals production, Biofuels. Bioproducts and Biorefining, 2012, 6: 580-598.

[2] Tian H,Jiao H,Cai J ,et al.Co-pyrolysis of Miscanthus Sacchariflorus and coals: A systematic study on the synergies in thermal decomposition, kinetics and vapour phase products. Fuel,2020, 262.

[3] Li R,Zhang J,Wang G ,et al.Study on CO_2 gasification reactivity of biomass char derived from high-temperature rapid pyrolysis. Applied Thermal Engineering, 2017, 121:1022-1031.

[4] Luo J,Lin L, Liu C,et al.Reveal a hidden highly toxic substance in biochar to support its effective elimination strategy. J Hazard Mater, 2020, 399, 123055.

[5] Abdullah H,Wu H.Biochar as a Fuel: 1. Properties and Grindability of Biochars Produced from the Pyrolysis of Mallee Wood under Slow-Heating Conditions. Energy & Fuels, 2009, 23: 4174-4181.

[6] Wang G,Zhang J,Chang W ,et al.Structural features and gasification reactivity of biomass chars pyrolyzed in different atmospheres at high temperature. Energy, 2018, 147:25-35.

[7] Tong W,Liu Q,Ren S ,et al.Effect of pyrolysis temperature on pine sawdust chars and their gasification reactivity mechanism with CO_2. Asia-Pacific Journal of Chemical Engineering,2018, 13.

[8] Gil M V,Riaza J,Álvarez L ,et al.Biomass devolatilization at high temperature under N_2 and CO_2: Char morphology and reactivity. Energy,2015, 91 :655-662.

[9] Rathnam R K,Elliott L K,Wall T F ,et al.Differences in reactivity of pulverised coal in air (O2/N2) and oxy-fuel (O_2/CO_2) conditions. Fuel Processing Technology, 2009, 90:797-802.

[10] Fan B-g,Jia L,Li B ,et al.Study on the Effects of the Pyrolysis Atmosphere on the Elemental Mercury Adsorption Characteristics and Mechanism of Biomass Char. Energy & Fuels, 2018, 32: 6869-6878.

[11] Zhang J,Liu J,Liu R.Effects of pyrolysis temperature and heating time on biochar obtained from the pyrolysis of straw and lignosulfonate. Bioresour Technol, 2015, 176: 288-91.

[12] Diao R,Zhu X,Wang C ,et al.Synergistic effect of physicochemical properties and reaction temperature on gasification reactivity of walnut shell chars. Energy Conversion and Management,2020, 204.

[13] Wang G,Zhang J,Shao J ,et al.Experimental and modeling studies on CO_2 gasification of biomass chars. Energy, 2016, 114: 143-154.

[14] Vincent S S,Mahinpey N,Aqsha A.Mass transfer studies during CO_2 gasification of torrefied and pyrolyzed chars. Energy, 2014, 67: 319-327.

[15] Hu Q,Yang H,Wu Z ,et al.Experimental and modeling study of potassium catalyzed gasification of woody char pellet with CO_2.Energy, 2019,171: 678-688.

[16] Kibria M A,Sripada P,Bhattacharya S.Steady state kinetic model for entrained flow CO gasification of biomass at high temperature. Energy, 2020, 196.

[17] Tian H,He Z,Wang J ,et al.Density Functional Theory Study on the Mechanism of Biochar Gasification in CO2 Environment. Industrial & Engineering Chemistry Research,2020 .

[18] Tian H,Hu Q,Wang J ,et al.Steam gasification of Miscanthus derived char: the reaction kinetics and reactivity with correlation to the material composition and microstructure. Energy Conversion and Management ,2020, 219.

[19] Fatehi H,Bai X-S.Structural evolution of biomass char and its effect on the gasification rate. Applied Energy,2017, 185: 998-1006.

[20] Wu Z,Yang W,Meng H ,et al.Physicochemical structure and gasification reactivity of co-pyrolysis char from two kinds of coal blended with lignocellulosic biomass: Effects of the carboxymethylcellulose sodium. Applied Energy, 2017, 207: 96-106.

[21] Zhang J,Guo J,Wang G,et al. Kinetics of petroleum coke/biomass blends during co-gasification, International Journal of Minerals. Metallurgy, and Materials,2016, 23:1001-1010.

[22] Dong Z,Yang Y,Cai W ,et al.Theoretical Analysis of Double Logistic Distributed Activation Energy Model for Thermal Decomposition Kinetics of Solid Fuels. Industrial & Engineering Chemistry Research, 2018, 57:7817-7825.

[23] Lin L,Strand M.Investigation of the intrinsic CO_2 gasification kinetics of biomass char at medium to high temperatures. Applied Energy, 2013, 109: 220-228.

[24] Ortega A. Some successes and failures of the methods based on several experiments. Thermochimica Acta, 1996, 284: 379-387.

[25] Criado J M,Ortega A.Kinetic study of thermal decomposition of dolomite by controlled transformation rate thermal analysis (CRTA) and TG. Journal of Thermal Analysis, 1991, 37: 2369-2375.

[26] Zhai M,Liu J,Wang Z,et al.Gasification characteristics of sawdust char at a high-temperature steam atmosphere. Energy,2017, 128: 509-518.

[27] He Q, Guo Q,Ding L, et al.CO_2 gasification of char from raw and torrefied biomass: Reactivity, kinetics and mechanism analysis. Bioresour Technol, 2019, 293:122087.

[28] Bai Y,Lv P,Li F, et al. Investigation into Ca/Na compounds catalyzed coal pyrolysis and char gasification with steam. Energy Conversion and Management, 2019, 184: 172-179.

[29] Gao M,Yang Z,Wang Y, et al.Impact of calcium on the synergistic effect for the reactivity of coal char gasification in H_2O/CO_2 mixtures. Fuel,2017, 189: 312-321.

[30] Huang Y,Yin X,Wu C, et al.Effects of metal catalysts on CO_2 gasification reactivity of biomass char, Biotechnol Adv,2009, 27: 568-72.

[31] Hu Y,Wang Z,Cheng X, et al. Non-isothermal TGA study on the combustion reaction kinetics and mechanism of low-rank coal char. RSC Advances, 2018, 41: 22909-22916.

[32] Chen J,Wang Y, Lang X, et al.Evaluation of agricultural residues pyrolysis under non-isothermal conditions: Thermal behaviors, kinetics, and thermodynamics. Bioresource Technology, 2017, 241: 340-348.

[33] Trubetskaya A, Jensen P A, Jensen A D ,et al. Influence of fast pyrolysis conditions on yield and structural transformation of biomass chars. Fuel Processing Technology, 2015, 140: 205-214.

[34] Apaydın-Varol E, Pütün A E. Preparation and characterization of pyrolytic chars from different biomass samples. Journal of Analytical and Applied Pyrolysis,2012, 98 : 29-36.

[35] Okuno T,Sonoyama N,Hayashi J , et al.Primary Release of Alkali and Alkaline Earth Metallic Species during the Pyrolysis of Pulverized Biomass. Energy & Fuels,2005, 19: 2164-2171.

[36] Tong W, Liu Q,Yang C ,et al.Effect of pore structure on CO_2 gasification reactivity of biomass chars under high-temperature pyrolysis. Journal of the Energy Institute. 2020, 93: 962-976.

[37] Hu Q,Yang H,Xu H ,et al.Thermal behavior and reaction kinetics analysis of pyrolysis and subsequent in-situ gasification of torrefied biomass pellets. Energy Conversion and Management,2018, 16: 205-214.

[38] Mollah M M, Jackson W R, Marshall M, et al. An attempt to produce blast furnace coke from Victorian brown coal. Fuel, 2015, 148:104-111.

[39] Sonibare O, Haeger T, Foley S F. Structural characterization of Nigerian coals by X-ray diffraction, Raman and FTIR spectroscopy. Energy,2010, 35: 5347-5353.

[40] Malekshahian M, Hill J M. Effect of Pyrolysis and CO_2 Gasification Pressure on the Surface Area and Pore Size Distribution of Petroleum Coke. Energy & Fuels,2011, 25: 5250-5256.

[41] Lahijani P, Zainal Z A, Mohamed A R, et al. CO_2 gasification reactivity of biomass char: catalytic influence of alkali, alkaline earth and transition metal salts. Bioresour Technol, 2013, 144: 288-295.

[42] Di Blasi C. Combustion and gasification rates of lignocellulosic chars. Progress in Energy and Combustion Science, 2009, 35: 121-140.

[43] Yip K, Ng E, Li C Z, et al. A mechanistic study on kinetic compensation effect during low-temperature oxidation of coal chars. Proceedings of the Combustion Institute,2011, 33:1755-1762.